An Automated Approach to Horn Antenna Impedance Matching and Manufacturing Using 3D Printing

Dorijan Sablić-Nemec, and Miroslav Joler, *Senior Member, IEEE*

***Abstract*—In this paper, we propose a streamlined design and automation of a horn antenna and its rectangular waveguide-based feeder using computer simulation-based optimizations and additive manufacturing. The approach enables time-effectiveness with a holistic design of the two components, while achieving advantageous results of the antenna parameters. The approach is described in comparison to other works and the results presented and discussed on the antenna models manufactured for two mid-band frequencies: at 2437 MHz and 5250 MHz. The optimum-search algorithm was able to find the parameter values that resulted in more than 25 dB improvement in S_{11}-parameter values in comparison to the initial design based on the textbook theory. For the 2437-MHz antenna, the achieved bandwidth, using the optimized parameters, was 16.52% wide comparing to 5.14% bandwidth that was the result based on the analytical expressions. In case of the 5250-MHz antenna, the optimized antenna bandwidth reached 25.47%. The fabricated antenna gain was close to the design value.**

***Index Terms*—horn antenna, additive manufacturing, impedance matching, 3D printing.**

I. Introduction

Fused filament fabrication (FFF), an additive manufacturing (AM) process, has come a long way from being a novel technology to becoming the default method of rapid manufacturing in the prototyping process of product design. In recent years, FFF and other AM processes have gained a lot of traction in numerous fields, since they require less space and power than traditional, older methods of manufacturing [1], such as Computer numerical control (CNC) milling or routing, while still delivering a sufficient performance of produced parts for many applications. The versatility of AM is best displayed by a collaborative project between NASA and Made In Space company [2], [3], where numerous functional tools were manufactured in space, utilizing a fused deposition modeling custom-made 3D printer, which is capable of printing in a zero-gravity environment [3].

Microwave engineering is one of the fields where AM has found its use in a variety of processes, such as in metamaterials [4] and millimeter-wave antenna development [5]. Many researchers have proven AM effectiveness [5]–[9], some on a traditional, simple structures, and other on highly challenging and complex metamaterial structures. Additive manufacturing of a horn antenna has been researched in a variety of papers [4]–[6], but the emphasis was mainly on the performance analysis [5], [10] in comparison to standard gain horns that were fabricated using conventional techniques.

The true potential of AM emerges from its synergy with parametric computer-aided design (CAD) methods. Parametric 3D modeling facilitates instantaneous design alterations by simply modifying input variables, thereby eliminating the need for manual redrawing.

The impedance of the adapter can be tuned by modifying the probe length and its position [11]–[13]. In [11], a series of experiments with waveguides was conducted in a search for an optimal backshort distance and probe length. In [13], numerical analyses were discussing the impact of the probe length, radius, and location within the waveguide adapter and the antenna was manufactured entirely by metal. In [14], [15] design optimization has been based on a parameter-tweaking approach, by tuning screws and posts. Because it is uncertain to connect a tuning post with the copper foil that is used to cover the surface of a 3D-printed antenna, such an approach is not the best choice for a 3D-printed structure. In [16], a full-wave numerical modeling of a probe-excited waveguide was proposed, but the work does not encompass a design of a horn antenna. In [17], a C-band adapter for a coaxial line-to-rectangular waveguide transition was analysed by simulations, with no horn antenna included in the work. Likewise, a design of a Chebyshev multi-section broadband coaxial-to-waveguide adapter was proposed in [18] for the THz regime, with 0.02-mm precision of fabrication but due to a multi-section design that increases the length, it would not be practical enough for an implementation with 3D printing at the S-frequency band. A recent publication that we found addressing fabrication of a horn antenna by means of additive manufacturing [19] did not, however, address a design of a horn with an integrated adapter and it also did not include an algorithm for a custom antenna design and optimization, but merely adopted the specifications of one commercial horn antenna just to test the feasibility of 3D printing for a horn antenna.

In contrast, a holistic computational approach for the design, optimization, and fabrication of horn antennas and their feeds is proposed in this paper, combining MATLAB™ [20] for the design and impedance matching, and Autodesk® Fusion

Manuscript received June 9, 2023; revised July 4, 2023. Date of publication July 27, 2023. Date of current version July 27, 2023.

D. Sablić-Nemec is with the Project Design department, Ericsson Nikola Tesla Servisi d.o.o., 10000 Zagreb, Croatia, email: dorijan.sablic-nemec@ericsson.com.

M. Joler is with the Department of Computer Engineering, Faculty of Engineering, University of Rijeka, 51000 Rijeka, Croatia, e-mail: mjoler@riteh.hr.

Digital Object Identifier (DOI): 10.24138/jcomss-2023-0100

360™ [21] for generating 3D printable models. This approach enables an automated, customized, time-efficient, cost-effective and light-weight design and fabrication of both the horn antenna and an integrated coaxial cable-to-rectangular waveguide adapter for feeding the antenna, by allowing a user to specify the design frequency of his preference rather than having to acquire a standardized off-the-shelf antenna designed for some of the IEEE frequency bands, which is a lot more costly and also may not be optimal for the user in some cases.

The algorithm is designed to require a minimal number of input variables, namely the design frequency, the desired antenna gain, and the feed probe diameter. Parametric 3D models for both the horn antenna and waveguide-to-coax adapter were created in Autodesk® Fusion 360™, with input variables corresponding to the outputs of the aforementioned MATLAB™ algorithm. This approach streamlines the generation of 3D printable models of the impedance-matched adapter and horn antenna.

Two mid-band frequencies were considered for the analysis and optimizations: 5250 MHz, to cover the 5-GHz 802.11ac Wi-Fi band from 32nd to 68th channel [22], and 2437 MHz to cover the first 11 channels of 802.11b/g/n Wi-Fi in the 2.4-GHz band [23].

Four antennas were fabricated for the two aforementioned frequencies. For each frequency, one of the antennas was designed in terms of the backshort distance and the probe feed length [11] by the streamlined procedure proposed in this paper, while the second antenna was manufactured using the dimensions defined by analytical expressions [24], [25]. The antennas were fabricated using polylactic acid (PLA) plastic and the FFF AM technology. A conductive layer that covers the inner surfaces of the antennas was applied by adhesion of a self-adhesive copper conductive tape. The antennas performance was then measured and compared against their traditionally designed counterparts in terms of the impedance bandwidth and antenna gain.

The paper is structured as follows: Section II describes the essential theory of the horn antenna and the feed structure and the textbook expressions applicable for a typical design. In Section III, the proposed impedance tuning algorithm is presented and the comparison between the results achieved by the classical design equations and the computer-based optimization are discussed. Section IV discusses our usage of additive manufacturing to fabricate the prototype antennas, while in Section V, we present and discuss the results of the measurements performed on the prototype antennas, showing the difference in the results achieved by the classically designed antennas vs. the computationally optimized 3D-printed antennas, as well as the difference between the measured results vs. the simulated results. Lastly, Section VII summarizes the paper.

II. Design and Analysis

A. Design of the Waveguide to Coaxial Adapter

A rectangular waveguide-to-coaxial adapter, shown in Fig. 1, in further text referred to as *the adapter*, is the common feeder of a pyramidal horn antenna and therefore the important point of the horn antenna design.

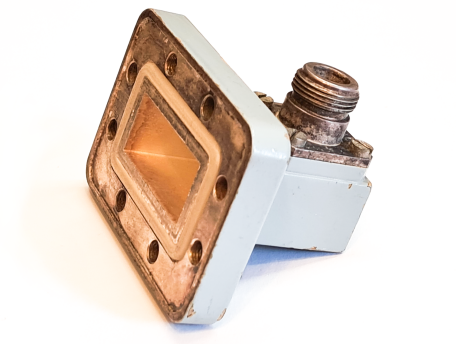

Fig. 1. A Commercial waveguide-to-coaxial adapter.

In the case of a rectangular waveguide, the dominant propagation mode is always TE_{10} [25], whilst the next propagation mode is not always the same, but can be obtained from the calculated cutoff frequency given by [25]

$$f_{c_{mn}} = \frac{1}{2\pi\sqrt{\mu\varepsilon}}\sqrt{\left(\frac{m\pi}{a}\right)^2 + \left(\frac{n\pi}{b}\right)^2} \tag{1}$$

$$\therefore$$

$$f_{c_{10}} = \frac{1}{2\pi\sqrt{\mu\varepsilon}}\sqrt{\left(\frac{\pi}{a}\right)^2} = \frac{1}{2a\sqrt{\mu\varepsilon}} \tag{2}$$

$$f_{c_{01}} = \frac{1}{2b\sqrt{\mu\varepsilon}} \tag{3}$$

$$f_{c_{11}} = \frac{1}{2b\sqrt{\mu\varepsilon}}\sqrt{1 + \left(\frac{b}{a}\right)^2} \tag{4}$$

$$f_{c_{20}} = \frac{1}{a\sqrt{\mu\varepsilon}} \tag{5}$$

From (1), (2), (3), (4), and (5), it is clear that TE_{01} mode will always have a lower cutoff frequency than TE_{11} mode, but not always lower than TE_{20} mode. If we now, for the sake of a further simplification, take that

$$f_{c_{20}} < f_{c_{01}} \tag{6}$$

by substituting (3) and (5) into (6), it leads to:

$$a > 2b \tag{7}$$

In further design and calculations, it will be assumed that condition (7) is met, in which case the TE_{20} mode will always follow the TE_{10} mode.

The center frequency of the adapter, f_c, is derived from (2) and (5) as:

$$f_c = \frac{\left(f_{c_{10}} + f_{c_{20}}\right)}{2} = \frac{3}{4a\sqrt{\mu\varepsilon}} = \frac{3c}{4a} \tag{8}$$

where $c = 3 \cdot 10^8$ m/s, is the speed of light in free space. From (8), the longer waveguide dimension a (Fig. 2) is obtained as

$$a = \frac{3\,c}{4f_c} \tag{9}$$

and, with the condition (7) satisfied, the shorter waveguide dimension b is calculated as

$$b_{max} = \frac{a}{2} \tag{10}$$

Keeping in mind that the antenna will be fabricated by an FFF 3D printer, the printing tolerances have to be kept in mind. Tolerances of a 3D printer [26] depend on many variables, which is why in this case, a safety margin of $tol = 0.6$ mm will be subtracted from dimension b, such that b does not exceed its maximal dimension given by (10). This particular value is here taken as a safety margin because it corresponds to a double of the declared precision tolerance [26] of the particular printer that will fabricate the antennas discussed in this paper, which is *Original Prusa MINI+* with a 0.4 mm extruder nozzle.

$$b \approx \frac{a}{2} - tol \tag{11}$$

B. Adapter Excitation Design

The preliminary analysis involved only the waveguide, but in order to design the adapter, several more parameters need to be defined.

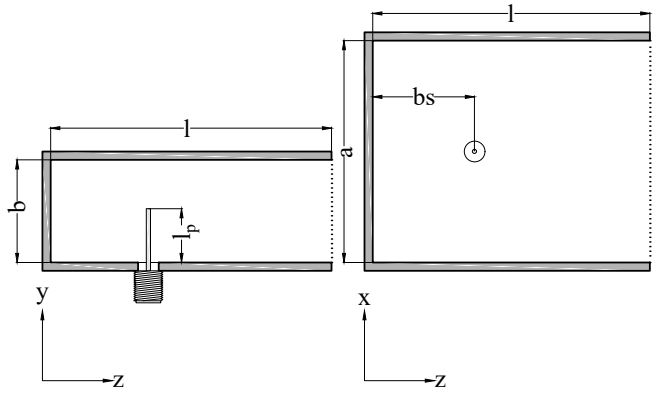

Fig. 2. A coax-to-waveguide adapter.

Figure 2 displays the geometry of the adapter and a monopole radiator (further referred to as the *probe*) being inserted into the waveguide that is shorted on one end. The distance from the center of the probe to the shorted end of the adapter, is referred to as the *backshort* distance, bs [11]. Traditionally, in the older references, it is advised that bs be exactly a quarter of a guided wavelength (λ_g) long, and the probe length (l_p) be equal to a quarter of the free space wavelength (λ_0) [11]. In [11], the said claim was investigated by a series of experiments, which proved that both l_p and bs directly impacted the SWR of the adapter. In the optimizations that are in the scope of this paper, the impact of l_p and bs will be further exploited wherein the quarter wavelength values, i.e. ($l_p = \lambda_0/4$ and $bs = \lambda_g/4$) are taken as a starting point for the design and optimizations. Regarding the adapter length (l), it is advised to be half of the guided wavelength long [27], i.e. $l = \lambda_g/2$.

The guided wavelength in a rectangular waveguide is calculated by [28]:

$$\lambda_g = \frac{\lambda_0}{\sqrt{1 - (\lambda_0/2a)^2}} \tag{12}$$

with a and b defined by (9) and (11), the adapter is further designed for the targeted center frequency using

$$\begin{aligned} l &= \frac{\lambda_g}{2} \\ bs &= \frac{\lambda_g}{4} \\ l_p &= \frac{\lambda_0}{4} \end{aligned} \tag{13}$$

C. Design of the Horn Antenna

The starting point of the design process for a pyramidal horn antenna is choosing the desired gain and calculating the adapter dimensions for the desired center frequency of the antenna. A horn antenna gain is defined by [13]

$$G = \frac{4\pi\, A_p\, e_A}{\lambda_0^2} \tag{14}$$

where A_p represents the antenna aperture, $A_p = A\,B$ and e_A is the aperture efficiency, which is best approximated with $e_A = 0.511$ [29] to achieve the optimal gain.

In this case, we chose to set the ratio of the adapter dimensions a and b, to be equal to the ratio of the respective horn dimensions, A and B, i.e.

$$\frac{a}{b} = \frac{A}{B} = x \tag{15}$$

When (15) is substituted into (14), it leads to

$$\begin{aligned} A &= \sqrt{\frac{G\,\lambda_0^2\,x}{4\pi\,e_A}} \\ B &= \sqrt{\frac{G\,\lambda_0^2}{4\pi\,e_A\,x}} \end{aligned} \tag{16}$$

With a calculated by (9) and b by (11), x is determined by (15) and A and B are readily computed by (16).

The horn lengths R_E and R_H in the E-plane and H-plane, respectively, are illustrated in Fig. 3 and defined by [24] as:

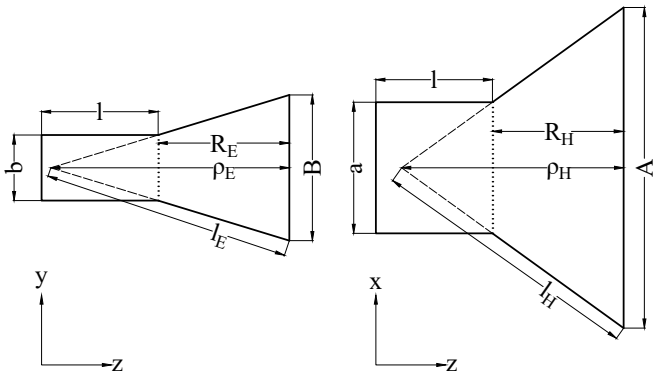

Fig. 3. A horn antenna slant lengths and the flare lengths in the E-plane and H-plane.

$$R_E = (B-b)\sqrt{\left(\frac{l_E}{B}\right)^2 - \frac{1}{4}}$$
$$R_H = (A-a)\sqrt{\left(\frac{l_H}{A}\right)^2 - \frac{1}{4}} \quad (17)$$

where l_E and l_H are the slant lengths of the horn in the E-plane and the H-plane, respectively.

It is understood that $R_E = R_H$ and further represented by a single term—the horn length in the propagation axis, R_P, as indicated in Fig. 4. In this design, R_P is chosen to be exceptionally short, and is approximated with $R_P \approx \lambda_0/3$. A similarly short horn design has also been proposed in [30].

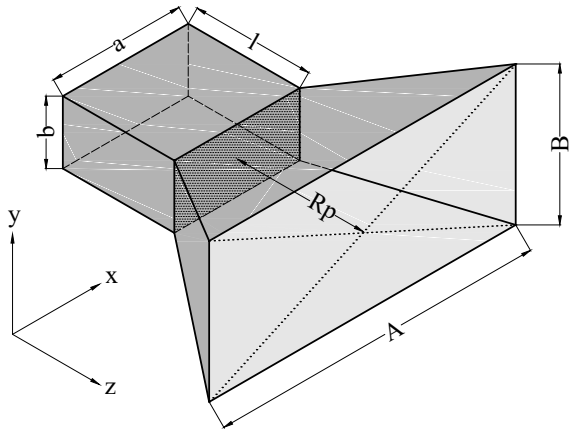

Fig. 4. A horn antenna.

For completeness, the slant lengths, l_E and l_H, can be derived from (17) as

$$l_E = B\sqrt{\left(\frac{R_E}{B-b}\right)^2 + \frac{1}{4}}$$
$$l_H = A\sqrt{\left(\frac{R_H}{A-a}\right)^2 + \frac{1}{4}} \quad (18)$$

while the focal lengths, ρ_E and ρ_H, based on the relations in Fig. 3, can be expressed as:

$$\rho_E = \sqrt{{l_E}^2 - \left(\frac{B}{2}\right)^2}$$
$$\rho_H = \sqrt{{l_H}^2 - \left(\frac{A}{2}\right)^2} \quad (19)$$

The summary of the antenna parameters, which were calculated according to the above procedure, is listed in Table I for the two chosen design frequencies, i.e. 2437 MHz and 5250 MHz. The diameter of the probe, which is one of the key inputs for the simulations in MATLAB™, was chosen to be 1.34 mm, while the desired antenna gain was arbitrarily chosen to be 10 dB.

TABLE I
DESIGN PARAMETERS CALCULATED BY ANALYTICAL EXPRESSIONS

Parameter	Center frequency, f_c	
	2437 MHz	5250 MHz
Waveguide width (a)	92.24 mm	42.81 mm
Waveguide height (b)	45.52 mm	20.81 mm
Waveguide length (l)	82.49 mm	38.29 mm
Aperture width (A)	218.55 mm	102.23 mm
Aperture height (B)	107.85 mm	49.68 mm
Flare length (R_p)	41.03 mm	19.05 mm
Backshort distance (bs)	41.25 mm $\approx \frac{\lambda_g}{4}$	19.15 mm $\approx \frac{\lambda_g}{4}$
Probe length (l_p)	30.75 mm$\approx \frac{\lambda_0}{4}$	14.28 mm$\approx \frac{\lambda_0}{4}$

III. IMPEDANCE MATCHING AND PARAMETER TUNING

The parameter tuning procedure is here based on a large number of simulations that were performed in MATLAB™, utilizing its computational electromagnetics features from the Antenna Toolbox™. The parameter tuning starts with the definition of the adapter's design frequency and dimensions as listed in Table I. All of the adapter and horn dimensions adopted from Table I were kept constant throughout the tuning process, while altering the backshort distance and probe length.

Unlike the approach in [11], tuning will not only be done with the waveguide-to-coax adapter in mind, but for both the horn antenna and the adapter. Moreover, in [11], the design tuning was performed by manual tweaking, while in this work, it was conducted entirely computationally.

The speed of the tuning algorithm is not of the primary concern in this case, so the algorithm will be based on the brute force approach, i.e. a large number of simulations being run before a superior solution is found.

SWR of the antenna will be simulated for all the given values of bs and l_p, and the lowest value of SWR will define the best combination of the input parameters. The brute force approach is not the fastest, but is immune to finding a suboptimal solution. This approach will produce a large dataset of antenna models and corresponding SWR values at the design frequency.

The algorithm, whose flowchart is shown in Fig. 5, was fed the initial values listed in Table I. The backshort distance was fed into the algorithm as an evenly spaced array of 100 values, starting with 20% of the initial backshort distance value, and ending with 180% of the initial value. The same was done with the probe length, but with the starting value set to 50% of the initial value, and the end value set at 100% of it. A total of 10,000 combinations of the backshort distance and the probe length were fed into MATLAB™'s Antenna Toolbox™. The simulations durations varied from a few minutes to about a half an hour. The resulting optimal values of the parameters are compared in Table II to the initial values obtained by the closed-form expressions from Section II. The values are listed both in the absolute values and as a fraction of the respective wavelength.

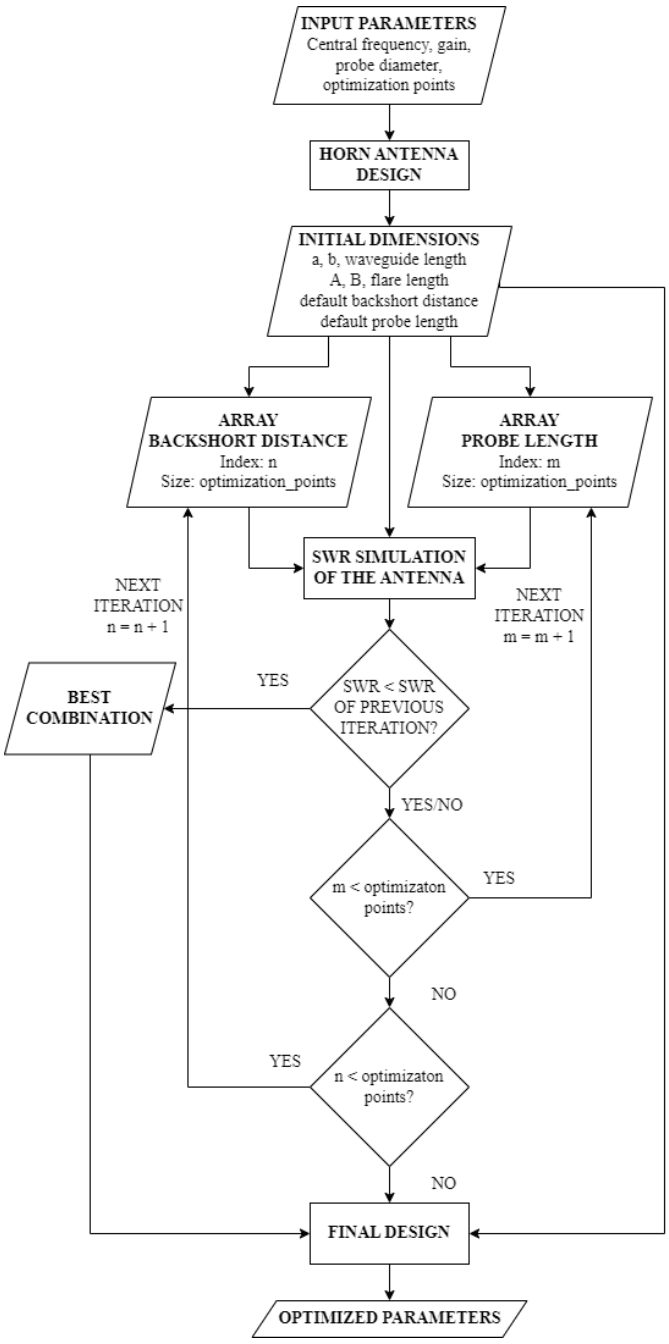

Fig. 5. Flowchart of the automated horn antenna design algorithm.

TABLE II
INITIAL VS. OPTIMIZED ANTENNA PARAMETERS

Parameter	Initial parameters		Tuned parameters	
	Center frequency		Center frequency	
	2437 MHz	5250 MHz	2437 MHz	5250 MHz
bs (mm)	41.25	19.15	27.55	12.45
bs (λ_g)	$\frac{\lambda_g}{4}$	$\frac{\lambda_g}{4}$	$0.67\ \frac{\lambda_g}{4}$	$0.65\ \frac{\lambda_g}{4}$
l_p (mm)	30.75	14.28	27.5	12.5
l_p, (λ_0)	$\frac{\lambda_0}{4}$	$\frac{\lambda_0}{4}$	$0.89\ \frac{\lambda_0}{4}$	$0.87\ \frac{\lambda_0}{4}$

It is noticeable that the algorithm chose both the backshort distance and the probe length to be shorter than the initial value. Percentile decrease in the backshort distance is 33% for the 2437 MHz antenna, and 35% for the 5250 MHz antenna. The probe length is decreased by 11% for the 2437 MHz antenna, and 13% for the 5250 MHz antenna.

For a better insight into the optimization results, each of the tuned antennas will be compared to its initial counterpart in terms of the reflection coefficient. The antenna designed for $f_c = 2437$ MHz will be analyzed in the range from 2 GHz to 3 GHz, with a resolution of 1000 frequency points, while the 5250-MHz antenna will be analyzed from 4.5 GHz to 7 GHz with the same frequency resolution. Table III shows the comparison of the reflection coefficient of the optimized design vs. the initial design in terms of the S_{11} frequency location and the value. The optimized antennas show noticeably better impedance matching near the design frequency, not only in terms of the reflection coefficient value, but also in the frequency location at which the minimum is found, which is substantially closer to the initially specified value. The difference is best seen by plots in Fig. 6.

TABLE III
SIMULATED S-PARAMETERS OF THE OPTIMIZED- VS. INITIAL- DESIGN

Design f_c	Set of parameters	Achieved f_c	$\lvert S_{11}\rvert$ at resonance
2437 MHz	initial	2375 MHz	-12.1 dB
	optimized	2436 MHz	-38.9 dB
5250 MHz	initial	5085 MHz	-11.35 dB
	optimized	5238 MHz	-48.56 dB

IV. ADDITIVE MANUFACTURING

Upon acquiring the tuned parameters, the antenna model was designed parametrically in Autodesk Fusion 360 computer-aided design (CAD) program [21]. Parametrical modeling enables this CAD model to be rapidly adapted to any change in the parameters of the antenna. All of the dimensions are expressed as variables, instead of absolute dimensions. This enables the CAD model to adapt to the variations in dimensions, without the need for manual redrawing.

A parametric CAD model, shown in Fig. 7, with dimensions adopted from Table II, was 3D-printed with an *Original Prusa MINI+* FFF 3D printer with Prusament PLA plastic [31] as a build material. The larger antenna, built for $f_c = 2437$ MHz, was 3D-printed with an *Original Prusa i3 MK3S* printer, because the *Original Prusa MINI+* printer does not have large enough a build surface. The extrusion nozzle used for the fabrication is a stock Prusa 0.4 mm brass nozzle. The CAD model was converted to a G-code [32] via Prusa Slicer software [33], with a 0.2-mm layer height, while the other key parameters (as in Table IV) were adopted from the Prusament PLA recommendations [31], which are listed on the packaging of the filament.

The printed parts were adhered with cyanoacrylate glue [34] and lined with copper self-adhesive conductive tape [35]. The adhesive material of the tape is electrically conductive, so the

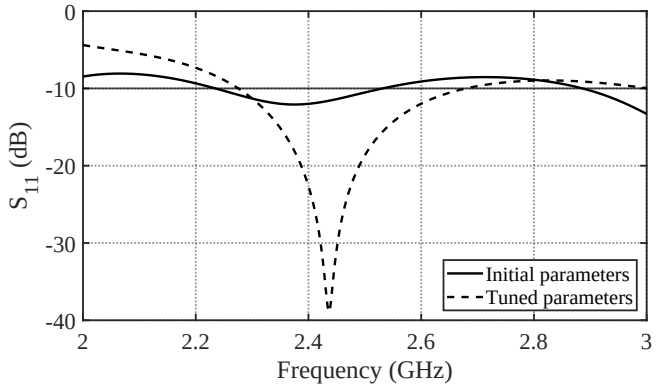

(a) Simulated S-parameters of the 2437 MHz antenna.

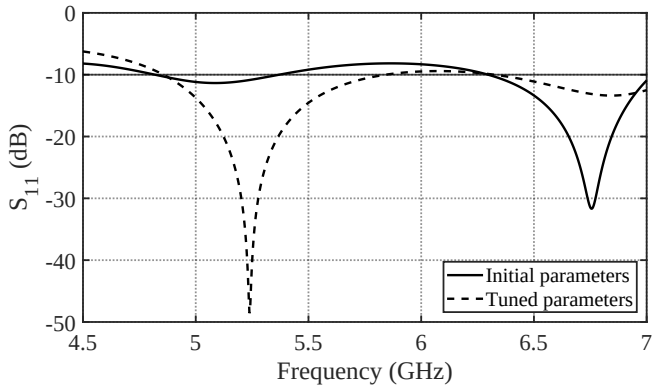

(b) Simulated S-parameters of the 5250 MHz antenna.

Fig. 6. Simulated S-parameters comparison of the tuned vs. initial antennas.

TABLE IV
PRUSAMENT PLA PRINTING PARAMETERS

Parameter	Recommended value
Nozzle temperature	210° C
Bed temperature	60° C
Print speed	200 mm/s

overlapping layers are electrically bonded and form a uniform conductive layer. This material has already been proven as an effective conductor in microwave circuits use cases [36], [37].

The probe was fabricated from a modified SMA connector, designed for soldering onto the printed circuit boards. A short probe of the SMA connector was cut, and a wire of 1.34-mm diameter was soldered onto it. After the soldering, the probe was cut to the length listed in Table II, and inserted into the adapter of the fabricated horn antenna.

Time of the manufacturing (Fig. 8) in case of the 5250-MHz antennas was 1 hour and 30 minutes for the adapter and 2 hours for the horn. In case of the 2437-MHz antennas, it took 6 hours and 30 minutes for the adapter and 9 hours for the horn. It was a time-consuming process, but justifiable because of wide availability of FFF printers and intervention-less process of printing which requires no operator presence once it is started.

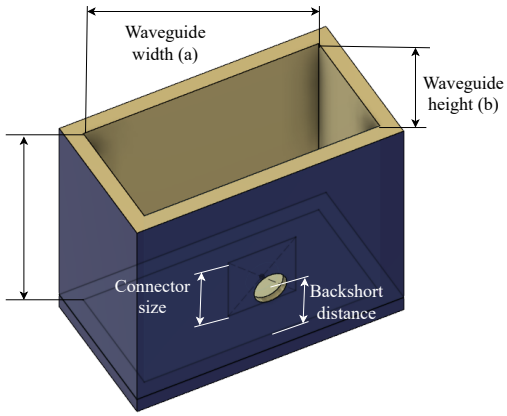

(a) Rendered CAD model of the adapter.

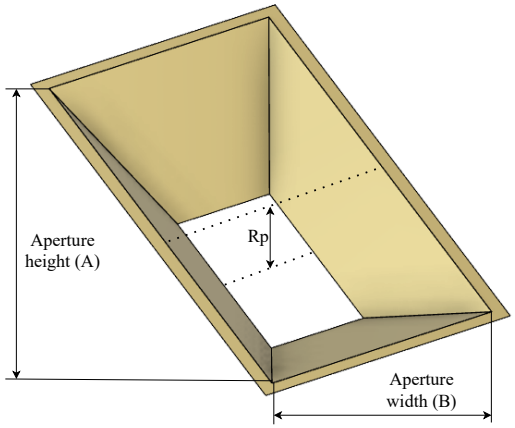

(b) Rendered CAD model of the horn.

Fig. 7. Parametric CAD models of the antenna parts.

V. MEASUREMENTS ON THE 3D-PRINTED ANTENNAS

A. The Impedance Bandwidth

After insertion of the SMA probe element, antennas displayed in Fig. 8 were measured using a MegiQ vector network analyzer (VNA) [38].

A comparison of the simulated vs. measured S-parameters of the initial- and optimized- 2437-MHz 5250-MHz antennas are shown in Figs. 9 and 10, respectively.

The results show that in the case of the antennas without parameter tuning, the measured S-parameter curve follows the simulated S-parameters, but with a deteriorated value of the reflection coefficient, which greatly worsens the antenna bandwidth. In case of the optimized antennas, the reflection coefficient is retained within acceptable limits, but the resonant frequency is somewhat downshifted in comparison with the simulations. This can be attributed to the imperfect fabrication (e.g. the adapter's probe) and can be improved by further adjustments in the circuit. For the 2437-MHz antenna, the usable bandwidth (BW) spans from 2.165 GHz to 2.555 GHz, which makes 16.52% of the fractional bandwidth (FBW) and is in excellent agreement with the simulated value, while for the 5250-MHz antenna, the BW spans from 4.186 GHz to 5.408 GHz, which achieves FBW=25.47% and exhibits a

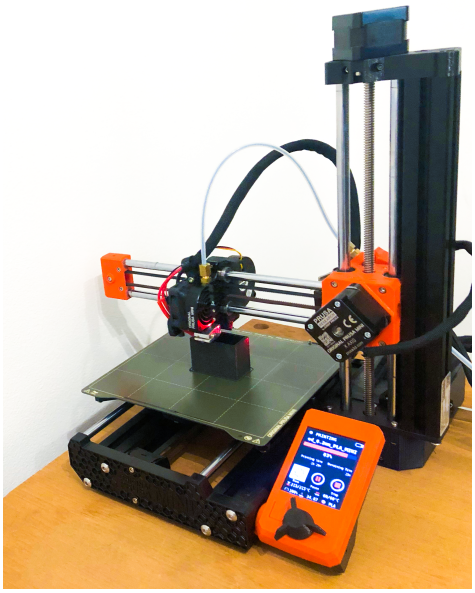

(a) 5250-MHz waveguide adapter in the printing process.

(b) Fabricated antennas.

Fig. 8. The additive manufacturing process.

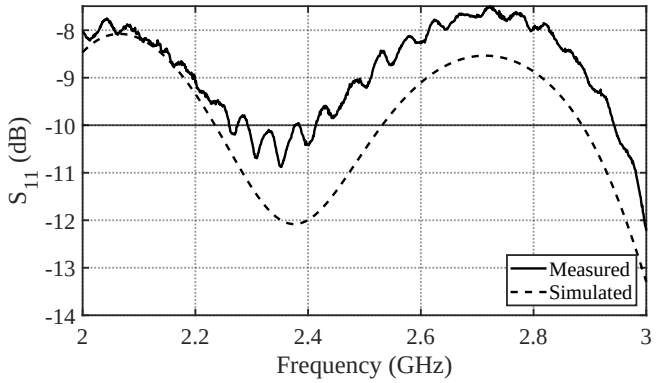

(a) 2437 MHz antenna without optimizations.

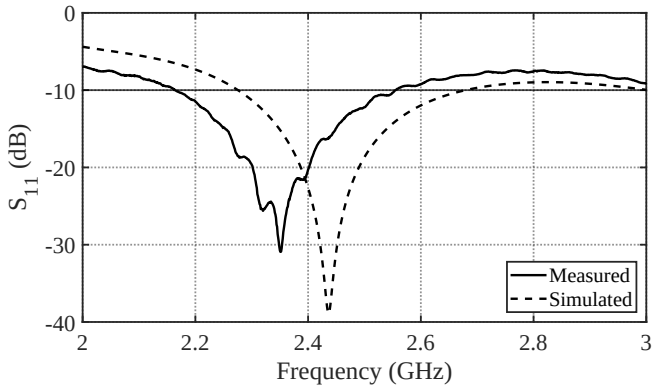

(b) 2437 MHz antenna with optimizations.

Fig. 9. Comparison of the simulated vs. measured S-parameters for the initial- and optimized- 2437-MHz antenna.

TABLE V
FRACTIONAL BANDWIDTH OF THE FABRICATED ANTENNAS

Design f_c	Set of parameters	FBW: simulated	FBW: measured
2437 MHz	initial	12.47%	5.14%
	optimized	16.23%	16.52%
5250 MHz	initial	10.76%	0%
	optimized	18.39%	25.47%

somewhat wider BW than the simulated antenna, due to a greater impact of the material losses. To get the resonant frequency of the 5250-MHz antenna closer to the design frequency, the inspection of the probe length showed that it was slightly longer than it had been specified by the calculation of the design parameters. After shortening its length to the value given in II, the achieved resonant frequency improved and came closer to the simulated curve, as shown in Fig. 11.

The fractional bandwidth (FBW) of all four antennas is listed in the Table V and shows that the fabricated antennas with the optimized parameters achieved substantially wider fractional bandwidths than the antennas designed with the analytical expressions in Section II. Wider FBWs of the fabricated antennas with respect to the simulated results is often the case because manufactured structures exhibit more imperfections and higher losses than the idealized computational models can assume.

B. The Radiation Patterns

Measurements of the radiation pattern were performed using the MegiQ Radiation Measurement System [39] and showed that the antennas had the gain value close to the value of 10 dB that was specified in the design phase. The simulated half-power beamwidth (HPBW) was 62° in the E-plane and 48° in the H-plane. The measured HPBWs of the 2437-MHz antenna were about 55° in both cut-planes, while for the 5250-MHz antenna, they were just slightly wider, with 65° in the E-plane and 55° in the H-plane.

The measured radiation pattern of the optimized antenna at 2437 MHz is shown in Fig. 12, while the comparison between the simulated and measured patterns in both cut-planes is shown in Fig. 13.

The measured radiation pattern measurement of the optimized antenna at 5250 MHz is shown in Fig. 14, while a com-

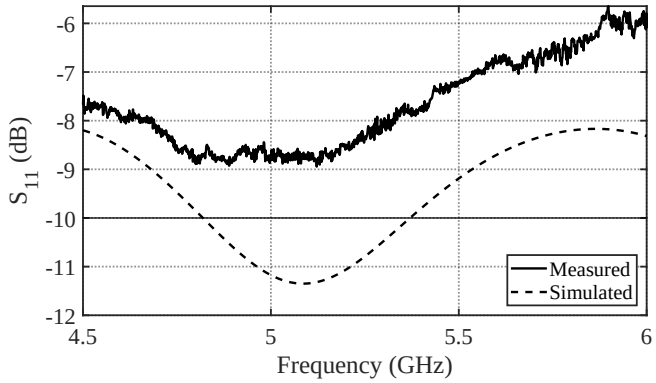

(a) The 5250-MHz antenna without optimizations.

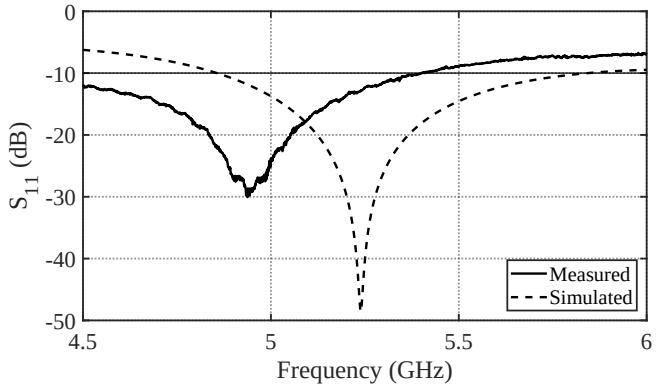

(b) The 5250-MHz antenna with optimizations.

Fig. 10. Comparison of the measured and simulated S-parameters for the 5250-MHz antenna.

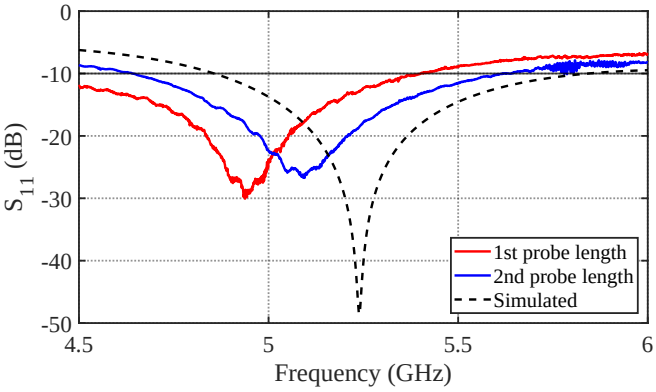

Fig. 11. A comparison of the improved resonant frequency of the 5250-MHz antenna after the probe length was corrected, i.e. shortened (here denoted as "2nd proble length".

parison between the simulated- and the measured- patterns in the E-plane and the H-plane is shown in Fig. 15, respectively. A good agreement between the simulated- and the measured-patterns is evident for both antennas.

The gain value within the usable bandwidth is shown in Fig. 16 for both antennas. A stable gain is observed over the entire useful BW, with a slight and typical increase of its value as the frequency increases. In the midband, the gain is slightly above 10 dB value that was targeted in the design. The simulated efficiency value indicated a bit too idealized value

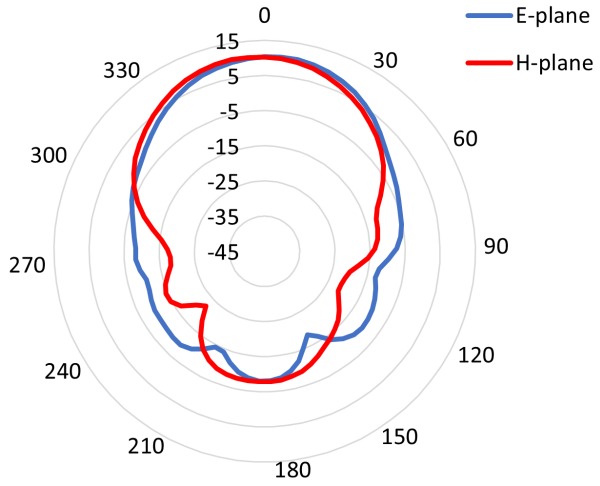

Fig. 12. Measured radiation patterns of the optimized antenna at 2437 MHz.

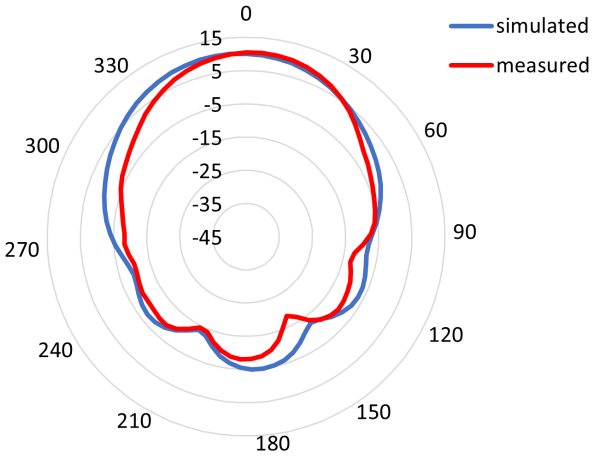

(a) E-plane

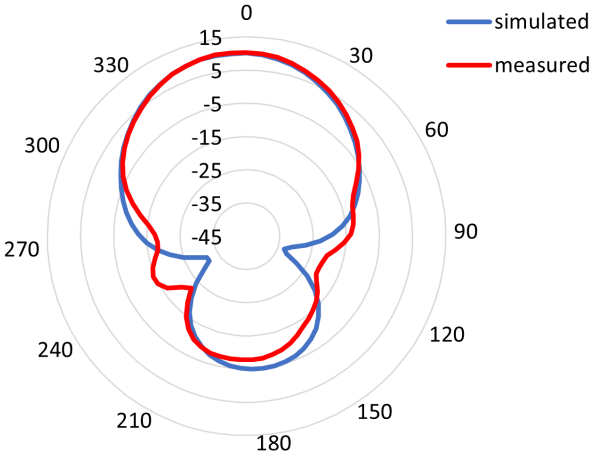

(b) H-plane

Fig. 13. Simulated vs. measured radiation patterns of the 2437-MHz antenna.

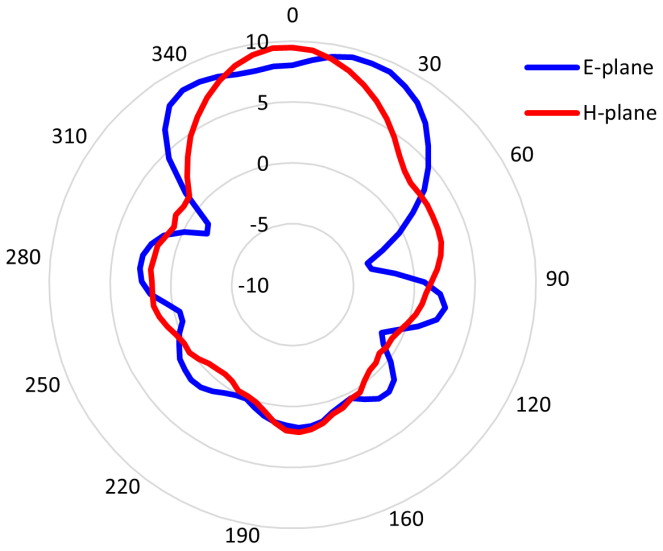

Fig. 14. Measured radiation patterns of the optimized antenna at 5250 MHz.

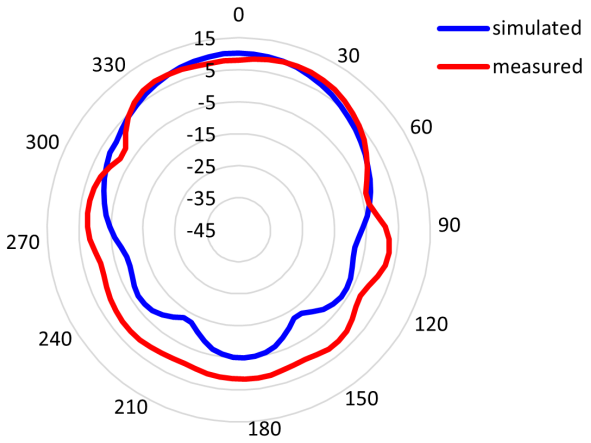

(a) E-plane

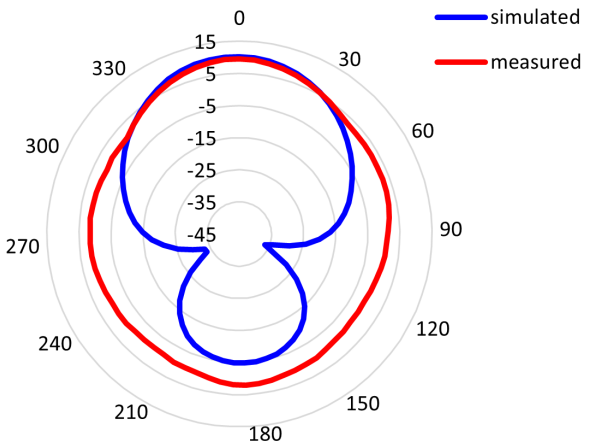

(b) H-plane

Fig. 15. Simulated vs. measured radiation patterns of the 5250-MHz antenna.

of 99.3%, while the measured efficiencies were above 90%, which is perhaps surprisingly impressive for a non-metal-made 3D-printed laboratory prototype antenna.

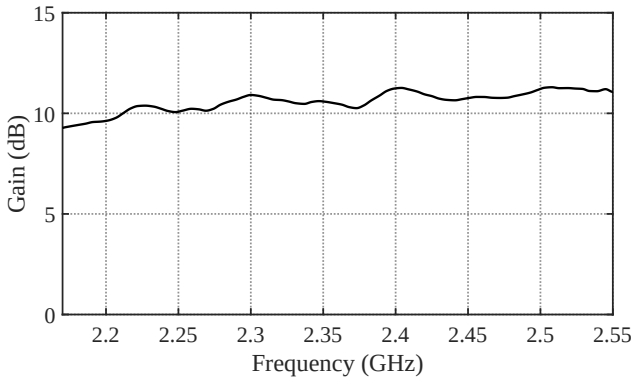

(a) 2437-MHz antenna

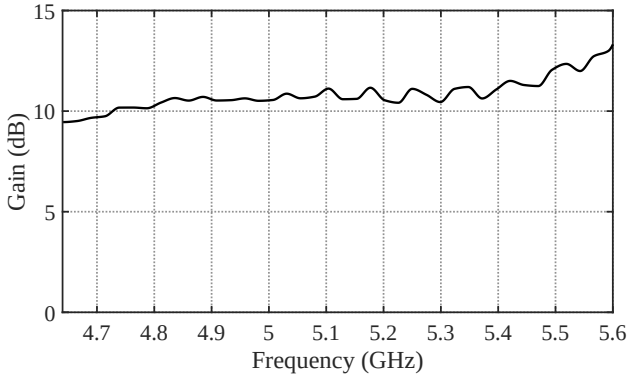

(b) 5250-MHz antenna

Fig. 16. The measured gain value versus frequency within the usable bandwidth of both manufactured antennas.

VI. Discussion

At this point, a comparison to some other references is useful. Among the recent works that we were able to find, the most pertinent reference to our work would be the one in [19], because it also used 3D printing of a model of horn antenna, albeit their horn was not a pyramidal horn, but an E-sector horn antenna. Regrettably, even though they utilized more expensive techniques to process the printed surface, such as the 3D print quality of 0.1 mm, galvanic plating using silver and 24-carat gold and using a microscopic inspection of the surface smoothness, we could find any particular value of gain, SWR and impedance bandwidth reported in the results of [19], while the radiation pattern and the denoted HPBW of the same cut-plane differed in the two subsequent figures. Apart from that, a comparison to some other references is here summarized in Table VI.

It is evident that our AM-based horn with an integrated adapter is very compact (see the *Total size* column) and lightweight, while offering a stable specified gain and high efficiency. Its bandwidth is somewhat narrower comparing to the metal-based horns, yet it fulfills the initial goal of covering the specified Wi-Fi bands of interest. The bandwidth

TABLE VI
A COMPARISON WITH REPORTED AM-BASED AND CONVENTIONAL METAL-BASED HORNS

Ref.	Material	Center freq. f_c	Adapter type	FBW (%)	Gain (dBi)	Horn dimensions (mm)			Total size (λ_0^3)	Effic. (%)	Weight, g
						A	B	Total length			
[13]	Metal	915 MHz	Integrated	52	8.4-12.6	450	320	360	1.47	72-80	-
[19]	AM	9.5 GHz	Separate	-	-	45	23	102	3.35	-	13
[40]	Metal	2.15 GHz	Separate	41.86	11	166	133.2	200	1.63	-	1526
[41]	Metal	5.975 GHz	Separate	35.98	11.2	61.4	49.3	118.1	2.82	-	266
[42]	Metal	0.95 GHz	Separate	52.63	11.2	454	328	671	3.17	-	8500
this	AM	2.44 GHz	Integrated	16.52	10.9	218.55	107.85	41.03	1.56	90.7	164
this	AM	5.25 GHz	Integrated	25.47	10.3	102.23	49.68	19.05	1.56	-	40

would probably be further improved implementing some of the following procedures: a) a more precise manufacturing, especially in the step of covering the surface with a conducting layer of higher quality and with a better accuracy; b) finding a more advantageous geometry of the horn; c) further optimizing the length and the radius of the feed probe; d) come up with a way to use a disc-ended probe that has proven to significantly extend the bandwidth [15], [17].

Overall, our prototypes show a good all-around performance in terms of the bandwidth, radiation patterns, gain, and efficiencies, yet being much lighter than the conventionally manufactured metal-based horns. In particular, a commercial 10-dB horn antenna (model WR-430 for 1.7 GHz–2.6 GHz) [40] weighs 861 g and the accompanying adapter weigh additional 664 g, both totaling to 1526 g. Contrary to it, our 2.4-GHz AM-based antenna with the integrated adapter weighs only 164 g, which is 10.75% of the weight of the referenced metal-based antenna. Likewise, another commercial 10-dB horn antenna, which comes with an adapter (model WR-159 for 4.9 GHz–7.05 GHz) [41] weighs total of 266 g, while our AM-based counterpart weighs only 40 g, which is 15% of the weight of the metal-based antenna.

Albeit the manufacturing accuracy of the AM process presents a greater uncertainty than working with standard metallic structures and CNC (Computer Numerical Control) machines, the presented results show that it is possible to make a satisfactory lightweight antenna at a low cost, with good radiation characteristics, but Fig. 17 illustrates how the result of the reflection coefficient may vary with an uncertainty in the actual value of the tolerance that is assumed for the 3D printer precision and is, as such, included in the design process. That being said, the two major goals of this work were met: a) to show a holistic approach to the design and manufacturing of both the horn antenna and an integrated impedance-matched probe-feed adapter; b) to make it feasible using AM.

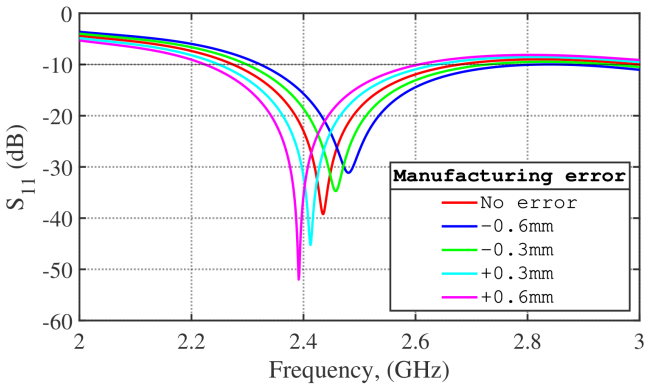

Fig. 17. Analysis of the impact of the printer nozzle error on the reflection coefficient.

VII. CONCLUSION

In this paper, we proposed an approach for a holistic design, optimization and additive manufacturing of a horn antenna with a feeder. We showed the improvement of the results with respect to the typical textbook-based theory and discussed the advantage of tackling the complete design by a parametric modeling and computational optimization that was finalized with a flexible 3D print of the system. The results were discussed in comparison to other references and showed the effectiveness. Such an approach simplifies the manufacturing process and enables cost-cutting, while achieving adequate results.

REFERENCES

[1] M. Kamran and A. Saxena, "A comprehensive study on 3D printing technology," *MIT Int J Mech Eng*, vol. 6, no. 2, pp. 63–69, 2016.
[2] N. Leach, "3D printing in space," *Architectural Design*, vol. 84, no. 6, pp. 108–113, 2014.
[3] M. J. Werkheiser, J. Dunn, M. P. Snyder, J. Edmunson, K. Cooper, and M. M. Johnston, "3D printing in Zero-G ISS technology demonstration," in *AIAA SPACE 2014 Conference and Exposition*, 2014, p. 4470.
[4] S. Zhang, D. Cadman, W. Whittow, D. Wang, G. Chi-Tangyie, A. Ghosh, A. Ketharam, A. Goulas, I. Reaney, B. Vaidhyanathan *et al.*, "3D antennas, metamaterials, and additive manufacturing," in *2019 IEEE MTT-S International Wireless Symposium (IWS)*. IEEE, 2019, pp. 1–3.
[5] B. Zhang, P. Linnér, C. Karnfelt, P. L. Tarn, U. Södervall, and H. Zirath, "Attempt of the metallic 3D printing technology for millimeter-wave antenna implementations," in *2015 Asia-Pacific Microwave Conference (APMC)*, vol. 2. IEEE, 2015, pp. 1–3.
[6] V. Midtbøen, K. G. Kjelgård, and T. S. Lande, "3D printed horn antenna with PCB microstrip feed for UWB radar applications," in *2017 IEEE MTT-S International Microwave Workshop Series on Advanced Materials and Processes for RF and THz Applications (IMWS-AMP)*. IEEE, 2017, pp. 1–3.
[7] M. Ferrando-Rocher, J. I. Herranz-Herruzo, A. Valero-Nogueira, and B. Bernardo-Clemente, "Performance assessment of gap-waveguide array antennas: CNC milling versus three-dimensional printing," *IEEE Antennas and Wireless Propagation Letters*, vol. 17, no. 11, pp. 2056–2060, 2018.

[8] A. T. Castro, B. Babakhani, and S. K. Sharma, "Design and development of a multimode waveguide corrugated horn antenna using 3D printing technology and its comparison with aluminium-based prototype," *IET Microwaves, Antennas & Propagation*, vol. 11, no. 14, pp. 1977–1984, 2017.
[9] B. J. Willis, *Compact form fitting small antennas using three-dimensional rapid prototyping*. The University of Utah, 2012.
[10] C. Garcia, R. Rumpf, H. Tsang, and J. Barton, "Effects of extreme surface roughness on 3D printed horn antenna," *Electronics letters*, vol. 49, no. 12, pp. 734–736, 2013.
[11] P. Wade, "Rectangular waveguide to coax transition design," *Qex*, vol. 8, pp. 10–17, 2006.
[12] M. Al-Hakkak, "Experimental investigation of the input-impedance characteristics of an antenna in a rectangular waveguide," *Electronics Letters*, vol. 5, no. 21, pp. 513–514, 1969.
[13] H. Kumar and G. Kumar, "Coaxial feed pyramidal horn antenna with high efficiency," *IETE Journal of Research*, vol. 64, no. 1, pp. 51–58, 2018.
[14] M. P. Weidman and E. Campbell, *A Method for Designing Multi-screw Waveguide Tuners*. US National Bureau of Standards, 1970, vol. 13.
[15] M. E. Bialkowski, "Analysis of a coaxial-to-waveguide adaptor including a discended probe and a tuning post," *IEEE Transactions on microwave theory and techniques*, vol. 43, no. 2, pp. 344–349, 1995.
[16] A. San Blas, F. Mira, V. Boria, B. Gimeno, G. Conciauro, M. Bressan, and P. Arcioni, "Efficient cad of generalized coaxial probes in rectangular waveguide using the 3d bi-rme method," in *2006 European Microwave Conference*. IEEE, 2006, pp. 1163–1166.
[17] V. V. Komarov, A. I. Korchagin, and V. P. Meschanov, "Broad-band coaxial-to-waveguide transition," in *2020 International Conference on Actual Problems of Electron Devices Engineering (APEDE)*. IEEE, 2020, pp. 163–165.
[18] D.-w. Song and G.-f. Zhao, "A novel design of 110 GHz broadband coaxial to waveguide adapter," in *2020 International Conference on Microwave and Millimeter Wave Technology (ICMMT)*. IEEE, 2020, pp. 1–3.
[19] J. Olivová, M. Popela, M. Richterová, and E. Štefl, "Use of 3D printing for horn antenna manufacturing," *Electronics*, vol. 11, no. 10, p. 1539, 2022.
[20] Mathworks. MATLAB. [Online]. Available: https://www.mathworks.com
[21] Autodesk. Fusion 360. [Online]. Available: https://www.autodesk.com/products/fusion-360/
[22] ETSI, "301 893 v2. 1.1 (2017-05) 5 GHz RLAN; harmonised standard covering the essential requirements of article 3.2 of directive 2014/53/eu," *Standard. Sophia Antipolis, France: ETSI*, 2017.
[23] ——, "300 328 v2. 2.2 (2019-07) wideband transmission systems; data transmission equipment operating in the 2.4 GHz band; harmonised standard for access to radio spectrum," *Standard. Sophia Antipolis, France: ETSI*, 2019.
[24] C. A. Balanis, *Antenna theory: analysis and design*. John Wiley & Sons, 2015.
[25] D. M. Pozar, *Microwave engineering*. John Wiley & Sons, 2011.
[26] Prusa Research. FAQ - frequently asked questions. [Online]. Available: https://help.prusa3d.com/article/faq-frequently-asked-questions_1932
[27] G. Banjeglav and K. Malarić, "2.4 GHz horn antenna," *Transactions on maritime science*, vol. 4, no. 01, pp. 35–40, 2015.
[28] R. F. R. Leighton and M. Sands, *The Feynman lectures on physics, v. 2*. Addison-Wesley Pub. Comp, 1964.
[29] T. Teshirogi and T. Yoneyama, *Modern millimeter-wave technologies*. IOS Press, 2001.
[30] K.-J. Lee, S.-S. Oh, Y.-H. Lee, and Y.-S. Kim, "Front-to-back ratio improvement of a short pyramidal horn antenna using metal strips/rods in lte/cellular band," *IET Microwaves, Antennas & Propagation*, vol. 10, no. 1, pp. 111–118, 2016.
[31] Prusa Research. Prusament PLA. [Online]. Available: https://prusament.com/materials/pla/
[32] G-code. G-code Explained. [Online]. Available: https://howtomechatronics.com/tutorials/g-code-explained-list-of-most-important-g-code-commands/
[33] Prusa Research a.s. Prusa slicer. [Online]. Available: https://www.prusa3d.com/page/prusaslicer_424/
[34] Henkel Corporation. LOCTITE® 406™ Instant Adhesive. [Online]. Available: https://www.henkel-adhesives.com/us/en/product/instant-adhesives/loctite_4060.html
[35] RS. A Complete Guide to Copper Tape. [Online]. Available: https://uk.rs-online.com/web/content/discovery/ideas-and-advice/copper-tape-guide
[36] F. Alimenti, P. Mezzanotte, M. Dionigi, M. Virili, and L. Roselli, "Microwave circuits in paper substrates exploiting conductive adhesive tapes," *IEEE Microwave and Wireless Components Letters*, vol. 22, no. 12, pp. 660–662, 2012.
[37] C. Mariotti, F. Alimenti, P. Mezzanotte, M. Dionigi, M. Virili, S. Giacomucci, and L. Roselli, "Modeling and characterization of copper tape microstrips on paper substrate and application to 24 GHz branch-line couplers," in *2013 European Microwave Conference*. IEEE, 2013, pp. 794–797.
[38] MegiQ. 6 GHz 3-port vector network analyzer. [Online]. Available: https://www.megiq.com/products/vna-0460e
[39] ——. 370 MHz to 6 GHz radiation measurement system. [Online]. Available: https://www.megiq.com/products/rms-0460
[40] Pasternack. WR-430 Standard Gain Horn Antenna Operating From 1.7 GHz to 2.6 GHz, 10 dBi Nominal Gain, CPR-430F Flange. [Online]. Available: https://www.pasternack.com/wr-430-waveguide-gain-horn-antenna-10db-cpr-430f-pewan430-10-p.aspx
[41] Pasternack. WR-159 Standard Gain Horn with 10 dBi gain, N Female connector. [Online]. Available: https://www.pasternack.com/wr-159-waveguide-standard-gain-horn-antenna-10-dbi-n-pewan159-10nf-p.aspx
[42] A-INFO. LB-975-10 0.75 - 1.12 GHz Standard Gain Horn Antenna. [Online]. Available: https://www.ainfoinc.com.cn/en/pro_pdf/new_products/antenna/Standard%20Gain%20Horn%20Antenna/tr_LB-975-10.pdf

Dorijan Sablić-Nemec received his B.Eng. degree in 2019 and his M.Eng. degree in 2023, both in electrical engineering from the University of Rijeka, Croatia. From 2021 to 2022, he was an Engineering Solution Designer, working on projects pertaining to fiber-optic networks, and since 2022, he has been a Project Solution Designer, working on 5G and FTTH rollouts, both with Ericsson Nikola Tesla Servisi d.o.o. company. His research interests include antennas, additive manufacturing, and process automation.

Miroslav Joler received his B.S. degree in electrical engineering from the University of Zagreb, Croatia, in 1996, and his M.S. and Ph.D. degrees in electrical engineering from the University of New Mexico, NM, USA, in 2001 and 2006, respectively. In 2006, he was a postdoctoral research associate at Portland State University, OR, USA. In 2007, 2013, and 2018, he was elevated to Assistant-, Associate-, and Full-Professor level at the Faculty of Engineering of the University of Rijeka, Croatia, respectively. In 2008, he also worked as Adjunct Assistant Professor with the Faculty of Maritime Studies of the University of Rijeka. Since 2008, he has served as the laboratory director, the Head of the Communications Systems Group, Graduation Committee Chair, and the department Chair. He has been a researcher in multiple scientific projects in the USA and Croatia, while his industry experience includes working as an RF engineer from 1996 to 1999. He has coauthored papers in distinguished scientific journals and conferences and served as a reviewer, technical- and international- program committee member, session (co-)chair and held invited conference talks. He has also served as a research proposal and annual report evaluator, editorial- or advisory- board member, an associate editor, and a guest editor of indexed journals. Prof. Joler is a Senior Member of the IEEE. In 2001, he received the University of New Mexico Graduate Office's Research, Proposal, and Travel Award. In 2017, he was admitted to the Associate level of Croatian Academy of Engineering. He has also received two Best Oral Presentation awards at international conferences. His research interests include antennas, smart clothing, wearable devices, self-recoverable systems, wireless power transfer, and biomedical applications of electromagnetics.